WATER RESOURCES RESEARCH, VOL. 32, NO. 7, PAGES 2021–2034, JULY 1996

Estimation of discharge from three braided rivers using synthetic aperture radar satellite imagery: Potential application to ungaged basins

Laurence C. Smith,[1] Bryan L. Isacks, and Arthur L. Bloom
Institute for the Study of Continents, Department of Geological Sciences, Cornell University, Ithaca, New York

A. Brad Murray[2]
Department of Geology and Geophysics, University of Minnesota, Minneapolis

Abstract. Analysis of 41 ERS 1 synthetic aperture radar images and simultaneous ground measurements of discharge for three large braided rivers indicates that the area of active flow on braided river floodplains is primarily a function of discharge. A power law correlation is found between satellite-derived effective width W_e and discharge Q, where W_e is the water surface area within a braided reach divided by the reach length. Synthetic values of W_e and Q generated from a cellular automata model of stream braiding display a similar power law correlation. Power functions that are fit through plots of W_e and Q represent satellite-derived rating curves that can subsequently be used to estimate instantaneous river discharge from space, with errors ranging from tens to hundreds of cubic meters per second. For ungaged rivers, changes in relative discharge can be determined from satellite data alone to determine the shape and timing of annual flows in glacierized basins. Absolute discharge can probably be estimated within a factor of 2. More accurate estimates will require either (1) one or more ground measurements of discharge acquired simultaneously with a satellite image acquisition, or (2) successful parameterization of known morphologic controls such as total sinuosity ΣP, valley slope, bank material and stability, and braid channel hydraulic geometry. Values of total sinuosity ΣP derived from satellite imagery and field measurements from two rivers of braid channel width, depth, velocity, water surface slope, and bed material grain size indicate that while the shape of satellite-derived W_e-Q rating curves may be influenced by all of these variables, the sensitivity of flow area to changing discharge is most dependent upon the degree of braiding. Efforts to monitor river discharge from space will be most successful for intensely braided rivers with high values of total sinuosity. Subsampling of existing daily discharge records from the Iskut River suggests that satellite return times of about 1 week are sufficient for approximating the shape and timing of the seasonal hydrograph in large, glacierized basins. Although errors are large, the presented technique represents the only currently available way to estimate discharge in ungauged braided rivers.

1. Introduction

Braided rivers contain multiple, shifting channels that widen and become more numerous in response to increased river discharge. Permanent gaging stations are impossible to install unless the braid channels coalesce into a single, semistable channel reach somewhere along the river. Braided rivers are particularly common in glacierized basins, and the paucity of streamflow data from such areas has hampered efforts to assess changes in meltwater production that may be occurring because of observed retreat of many of the world's alpine glaciers [*Meier*, 1984; *Haeberli et al.*, 1989]. Streamflows are also virtually unknown in remote areas such as the north slope of Alaska and southwest Greenland, where conditions are hostile and most rivers are braided. The need for quantitative characterization of the hydrological regime of such regions has become more urgent, as general circulation model (GCM) experiments predict amplification of a greenhouse gas-induced increase in global temperature at high latitudes [*Manabe and Wetherald*, 1980; *Manabe et al.*, 1991; *Mitchell et al.*, 1995]. The timing and volume of streamflow in such basins are also minimum requirements for assessing hydroelectric potential and water supply, yet this information is lacking for most high-latitude braided rivers in North America.

For over 20 years, satellites operating in the visible and near-infrared range of the electromagnetic spectrum have been used to map flood inundation areas around rivers [*Halberg et al.*, 1973; *Rango and Anderson*, 1974; *Morrison and White*, 1976; *Kruus et al.*, 1981; *Berg et al.*, 1981; *Brooner and Binaghi*, 1983; *Barton and Bathols*, 1989; *Pope et al.*, 1992; *Blasco et al.*, 1992]. However, active and passive microwave sensors are also sensitive to open water surfaces and are superior to visible and near-infrared sensors for multitemporal

[1]Permanently at Department of Geography, University of California, Los Angeles.
[2]Permanently at Scripps Institution of Oceanography, University of California, San Diego, La Jolla.

Paper number 96WR00752.
0043-1397/96/96WR-00752$09.00

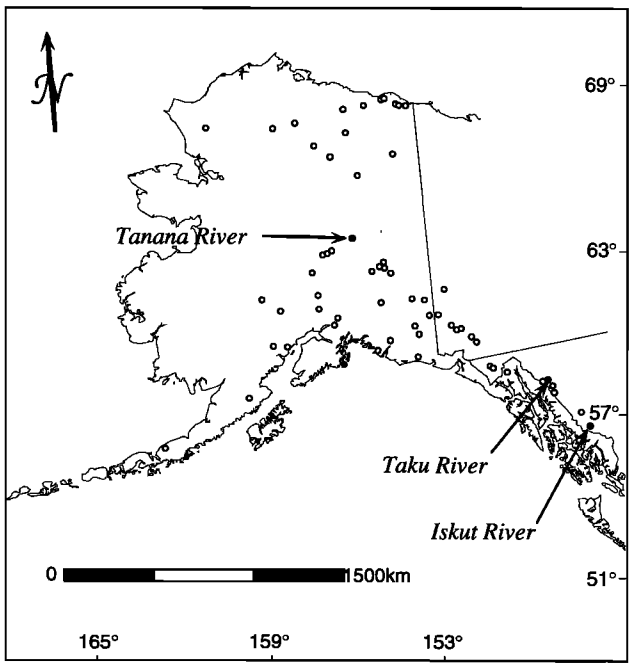

Figure 1. Location of the Tanana, Taku, and Iskut Rivers. Locations of prominent braided reaches on 55 other large rivers in Alaska, northwest British Columbia, and the southwestern portion of the Yukon Territory are also shown.

studies due to their all-weather, day/night capability. Microwave remote sensing may well be the only way to monitor changing river conditions in remote and chronically cloudy regions such as the Coast Range of Alaska and British Columbia. Passive microwave sensors are limited by spatial resolutions of about 25 km (at 37 GHz) but have successfully been used to monitor very large flooded regions in Australia and South America [*Allison et al.*, 1979; *Choudhury*, 1991; *Sippel et al.*, 1994; *Hamilton et al.*, 1996]. Active radars have been used to map flood inundation boundaries in Bangladesh [*Imhoff et al.*, 1987] and Europe [*Blyth and Biggin*, 1993; *Noyelle et al.*, 1995; *Kannen*, 1995; *Tholey*, 1995; *Chalah et al.*, 1995] and can even detect river flooding beneath forest canopies [*Ormsby et al.*, 1985; *Richards et al.*, 1987; *Sippel et al.*, 1992; *Hess and Melack*, 1994]. *Hess et al.* [1995] used a decision-tree model to classify multiparameter synthetic aperture radar (SAR) data acquired over the Negro and Amazon Rivers during the 1994 Spaceborne Imaging Radar (SIR-C) experiments. C band (5.7 cm) and L band (24 cm) wavelengths were used to distinguish open water, pasture, floating meadow, flooded forest, and nonflooded forest. *Hess et al.* [1990] and *Melack et al.* [1994] provide comprehensive reviews of the interaction of various radars with a wide range of flooded vegetation types. More general reviews of river remote sensing are provided by *Hockey et al.* [1990] and *Smith* [1996].

Efforts have recently been made to obtain measurements of river stage and discharge from space. Radar altimeter waveform data have been used to measure river stage in the Amazon [*Koblinsky et al.*, 1993], while *Brakenridge et al.* [1994] combined First European Remote Sensing Satellite (ERS 1) synthetic aperture radar images with high-resolution topography to determine water-edge elevations along the Mississippi River during the "Great Flood" of 1993. This method has also been used with Landsat data to estimate water volume in reservoirs [*Gupta and Banerji*, 1985]. Our own preliminary study of the braided Iskut River in British Columbia, Canada, first suggested that ERS SAR data may be used to estimate instantaneous discharge from the total water surface area contained within a braided reach [*Smith et al.*, 1995]. To develop this approach further, we now (1) present ERS 1-derived effective width/discharge rating curves for three braided rivers in Alaska and British Columbia, (2) relate morphologic and hydraulic field measurements from two of these rivers to the SAR data, (3) present the nonlinear relationship between effective width and discharge generated from a cellular automata model of stream braiding, (4) show examples of the usefulness of SAR images for monitoring other river conditions besides discharge, and (5) discuss requirements for application of this technique to ungaged braided rivers.

2. Location of Study Sites: Tanana, Taku, and Iskut Rivers

Correlations between satellite-derived water surface area and ground measurements of discharge were determined for the Tanana, Taku, and Iskut Rivers in Alaska and British Columbia (Figure 1). ERS 1 synthetic aperture radar images were acquired over these sites in 1992 and 1993 by the Alaska SAR Facility, Fairbanks. These rivers are relatively large (flows are of the order of 1000 m^3/s) and unusual in that they are intermittently braided along their lengths. This characteristic has permitted installation of permanent gaging stations 5–18 km downstream of large braided sections that may be monitored by satellite. Ground measurements of daily mean discharge from the Tanana and Taku Rivers were collected by the U.S. Geological Survey, Water Resources Division. Hourly data for the Iskut River were provided by the Water Survey of Canada and were averaged to a 24-hour mean value for comparison with satellite-derived measurements of inundation area. Day-to-day discharge variations in these large rivers are small (~1–6% for the Tanana River; ~3–6% for the Taku River), as are hourly variations within a 24-hour period for the Iskut River (~5%). For this reason, daily mean ground measurements of discharge were compared directly with instantaneous satellite observations of water surface area in braided reaches upstream of the gauging stations. No flow routing or other time lag correction was applied to the ground discharge data.

The locations of 59 prominent braided reaches from 55 other rivers in Alaska and Canada are also shown in Figure 1. They represent potential future sites for application of this discharge estimation technique and were located from a systematic search of topographic maps from northwest British Columbia, the southwest Yukon Territory, and Alaska.

3. Spaceborne Synthetic Aperture Radar Sensors

Synthetic aperture radar remote sensing offers two major advantages over the visible and near-infrared range for applications in hydrology: (1) SAR can penetrate clouds and darkness, and (2) active microwaves are strongly sensitive to the presence of liquid water, whether in a soil media (where an increased complex dielectric constant enhances backscattering to the satellite) or in a smooth open body (which specularly reflects incident microwaves away from the satellite). The complex dielectric constant of a material is proportional to the

strength of its dipole moment in the presence of a time-varying external electric field. When a surface is subjected to an incident microwave, the ratio of incident energy reflected away from the surface to the energy refracted downward into the media is proportional to the dielectric constant and the local incidence angle. The angular radiation pattern reflected by a surface is determined by the surface roughness (on the scale of the microwave wavelength) and local slope, which exerts a net directionality to the radiation pattern. Normalized radar backscatter σ° returned to the satellite from most natural surfaces is thus a function of the surface roughness, topography, and moisture content.

The ERS 1 satellite was launched on July 17, 1991, by the European Space Agency and has provided all of the SAR data presented here. The anticipated successor ERS 2 was launched on April 20, 1995. Both operate at C band (5.3 GHz) with vertical transmit and receive (VV) polarizations, producing an 80- to 103-km swath with a nominal spatial resolution of 25 m and a processed pixel spacing of 12.5 m. The Canadian RADARSAT, launched on November 4, 1995, also uses a C band (5.3 GHz) SAR but with horizontal transmit and receives (HH) polarizations. RADARSAT offers a special high-resolution mode with a 9-m spatial resolution that should be particularly useful for this discharge estimation application.

4. ERS 1 SAR Data Processing Procedures

Forty-one ERS 1 SAR images acquired over the Tanana, Taku, and Iskut Rivers by the Alaska SAR Facility were used to determine the correlation between active flow area and discharge in 1992 and 1993 (Table 1). Two closely related river flow parameters, effective width W_e and total sinuosity ΣP, were derived from each ERS 1 image. Values of W_e were computed following three processing steps (radiometric calibration, classification, and majority filtering). Values of ΣP were obtained after two additional steps (refiltering and link fitting). These five processing steps are described next and illustrated with an example from the Iskut River in Figure 2.

4.1. Water Surface Area

Radiometric calibration of each image was done with Alaska SAR Facility software to permit comparison of σ° between multitemporal images and also within a single scene (Figure 2a). The calibration process removes variations in σ° caused by sensor antenna pattern, range to target, and incidence angle for each image, using a satellite-derived noise versus range function and three calibration coefficients [*Bicknell*, 1992].

Heavily braided reaches from 9 to 16 km in length were selected as control sections for the Tanana, Taku, and Iskut Rivers. In addition, three sections were defined at different locations along the Tanana River to assess the influence of channel morphology upon the slope of satellite-derived effective width/discharge rating curves. A threshold approach similar to that of *Chalah et al.* [1995] was used to classify the open water surface. For each ERS 1 SAR image an upper threshold of −10.5 dB was used for classification of the data as "water" or "not water" (Figure 2b). As discussed previously [*Smith et al.*, 1995], this value appears to work well for classifying open water on braided rivers. Thresholds set lower than −10.5 dB tend to miss some water surface area; higher thresholds classify noncontiguous patches that are probably not channels.

A 3 × 3 bimodal majority filter was next applied to each classified image to reduce speckle (Figure 2c). The eight neighbors surrounding each pixel are evaluated to determine whether the center pixel is isolated and anomalous; in which case it is considered to be speckle and is assigned the value of a majority of its neighbors. This approach is similar to that of *Kellndorfer et al.* [1993]. Total water surface area is then computed as the area of the remaining classified pixels. Effective width W_e is obtained by dividing this water surface area by the length of the control section. Although W_e has units of length, it represents inundation area and can be thought of as the total width per unit length of all braid channels in the control section.

Table 1. Orbit Numbers and Greenwich Meridian Time Dates of Acquisition for the 41 ERS 1 Synthetic Aperture Radar Scenes Used to Produce Figure 3

Orbit	Date	Q, m³/s	W_e, m	ΣP	Q_p-Q, m³/s
		Iskut River			
04424	May 20, 1992	292	437	6.39	307
04696	June 8, 1992	951	579	7.75	97
05197	July 13, 1992	1570	656	9.48	−225
05426	July 29, 1992	1110	584	8.17	−44
05698	Aug. 17, 1992	862	490	6.39	−111
06199	Sept. 21, 1992	735	393	4.82	−250
06428	Oct. 7, 1992	388	291	2.04	−122
06929	Nov. 11, 1992	164	261	3.30	50
09434	May 5, 1993	370	316	5.01	−57
09706	May 24, 1993	1320	621	8.58	−112
09935	June 9, 1993	1140	596	8.28	−28
10207	June 28, 1993	948	498	6.49	−172
10436	July 14, 1993	1080	694	10.12	425
10708	Aug. 2, 1993	1121	533	7.24	−231
10937	Aug. 18, 1993	818	534	7.02	76
11209	Sept. 6, 1993	681	446	5.54	−58
11438	Sept. 22, 1993	235	311	3.71	69
11710	Oct. 11, 1993	266	294	3.29	6
12211	Nov. 11, 1993	403	381	3.96	53
		Taku River			
04052	April 24, 1992	277	301	4.92	−15
04281	May 10, 1992	436	358	4.03	−11
04782	June 14, 1992	1840	541	6.33	−487
05054	July 3, 1992	1840	520	5.54	−633
05555	Aug. 7, 1992	801	360	3.61	−368
05991	Sept. 7, 1992	309	229	1.99	−187
06285	Sept. 27, 1992	221	339	3.44	145
06557	Oct. 16, 1992	136	288	2.61	95
06786	Nov. 1, 1992	124	290	3.00	113
09770	May 29, 1993	1480	574	6.14	111
15099	June 5, 1994	765	491	5.06	264
		Tanana River			
4568	May 30, 1992	1764	820.2	10.41	−297
5069	July 4, 1992	1617	782.1	9.61	−315
5799	Aug. 24, 1992	1158	733.3	8.98	−51
6071	Sept. 12, 1992	595	562.2	12.27	−26
6300	Sept. 28, 1992	445	494.4	6.42	−33
6572	Oct. 17, 1992	283	407.9	4.43	−29
9306	April 26, 1993	566	614.6	8.04	144
9807	May 31, 1993	1000	704.8	8.30	3
10308	July 5, 1993	1413	825.9	11.14	80
10809	Aug. 9, 1993	1586	857.7	12.10	56
11310	Oct. 19, 1993	561	649.1	9.88	254

Satellite-derived values of effective width (W_e) and total sinuosity (ΣP) are shown, as well as ground discharge measurements (Q) for the Iskut, Tanana, and Taku Rivers. Differences between the predicted discharge (Q_p) based on best fit power functions and actual discharge Q are also shown.

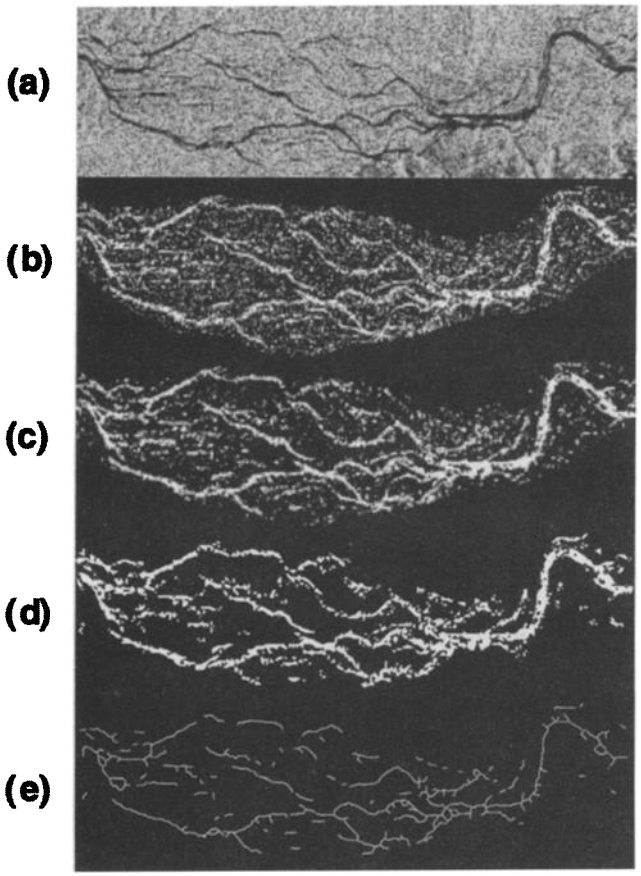

Figure 2. Processing procedure for ERS 1 SAR data, Iskut River, British Columbia: (a) radiometric calibration, (b) water classification, (c) speckle filtering, (d) cluster removal, and (e) link fitting. Effective width W_e is computed following steps in Figures 2a, 2b, and 2c. Steps in Figures 2d and 2e are required to obtain total sinuosity ΣP. Braid complex is approximately 10 × 3 km.

4.2. Total Sinuosity

The degree of braiding varies along a river's length and also differs between rivers. Clearly, the sensitivity of water surface area to changing discharge is influenced by the intensity of braiding. With increasing discharge an incised meandering river will experience little widening (until its banks are overtopped), while an intensely braided river will increase its flow area continuously. The major reason for this effect is that meandering rivers tend to have steeper and more stable banks than braided rivers, owing to the presence of cohesive sediment and vegetation cover. In order to characterize the intensity of braiding for each control section used in this study a total sinuosity index ΣP was calculated from each SAR image acquired over the control sections. ΣP is defined as the cumulative length of all braid channels in a reach divided by the reach length [*Hong and Davies*, 1979; *Robertson-Rintoul and Richards*, 1993]. Like effective width, total sinuosity is a function of discharge; for most natural rivers there is no single value of ΣP that exists at all states of discharge.

To obtain values of ΣP from the ERS 1 data, each classified image was refiltered to remove all clusters of noncontiguous pixels. All pixel groupings classified as water that could be fully contained within a 10 × 10 window were removed (Figure 2d), permitting large oblong or linear features to remain. Next, a network of links was fit through the remaining classified pixels as an approximation of the braid channel network (Figure 2e). The sum of all link lengths was then divided by the control section length to obtain the total sinuosity index for that date. Filtering, link fitting, and link summation were accomplished using standard ARC/INFO (v. 7.0) library routines.

The values of ΣP yielded from SAR data may not be the same as those obtained from air photographs of a braided river. The 25-m nominal spatial resolution imposed by the ERS 1 Active Microwave Instrument fails to adequately resolve small channels, causing gaps to occur in the derived braid channel network. This problem is offset by nature of the edge-detection algorithm utilized by ARC/INFO, which attempts to fit channel widenings with very short links that spur away from the main trunk link. Although they do not represent true channels, the lengths of these additional short links are included in the link summation calculation, mitigating length losses due to gaps. However, use of an automated line-fitting procedure was determined to be comparable to line fitting by eye but considerably less time-intensive. Values of ΣP produced by manual line fitting for six ERS 1 SAR images were all within 15% of the corresponding values generated by the automated procedure.

5. Results

5.1. Discharge Estimation

A total of 72 ERS 1 SAR images were acquired over the Tanana, Taku, and Iskut Rivers in 1992 and 1993. Twenty-four of the images were rejected for processing because of the presence of river ice, as there is no unique relationship between river ice area and instantaneous discharge. An additional seven images were discarded because of strong wind or wet gravel at the time of image acquisition (see section 7). Values of effective width W_e and total sinuosity ΣP derived from the remaining 41 SAR images are presented with ground measurements of discharge Q in Table 1. The correlations between W_e and Q for the Tanana, Iskut, and Taku Rivers are plotted in Figure 3. Best fit power functions are $W_e = 50.45Q^{0.38}$ ($R^2 = 0.91$), $W_e = 29.89Q^{0.42}$ ($R^2 = 0.84$), and $W_e = 72.31Q^{0.26}$ ($R^2 = 0.74$) for the Tanana, Iskut, and Taku Rivers, respectively. Regression of log Q on log W_e yields $Q = 7.03 \times 10^{-5} W_e^{2.51}$, $Q = 3.19 \times 10^{-3} W_e^{2.00}$, and $Q = 3.18 \times 10^{-5} W_e^{2.80}$, respectively. These power functions represent satellite-derived rating curves which relate the area of active flow to discharge. Once established, they may be used to estimate river discharge from satellite measurements alone. Departures (in cubic meters per second) of ground discharge measurements from the values predicted by these power functions are listed for each satellite data acquisition in Table 1. Errors range from tens to hundreds of cubic meters per second, with many (but not all) of the largest errors associated with high-discharge conditions. Despite observed changes in channel configuration and a major flood event on the Iskut River the W_e-Q rating curves remained stable throughout two melt seasons. Potential changes in the W_e-Q relationship induced by a shifting braid channel configuration appear to be avoidable if control sections of the order of 10 km in length are chosen, most likely from spatial averaging of these small-scale effects.

5.2. Effect of Channel Morphology on W_e-Q Rating Curves

Within a 35-km transition zone the Tanana River changes from a highly braided to nearly meandering channel morphol-

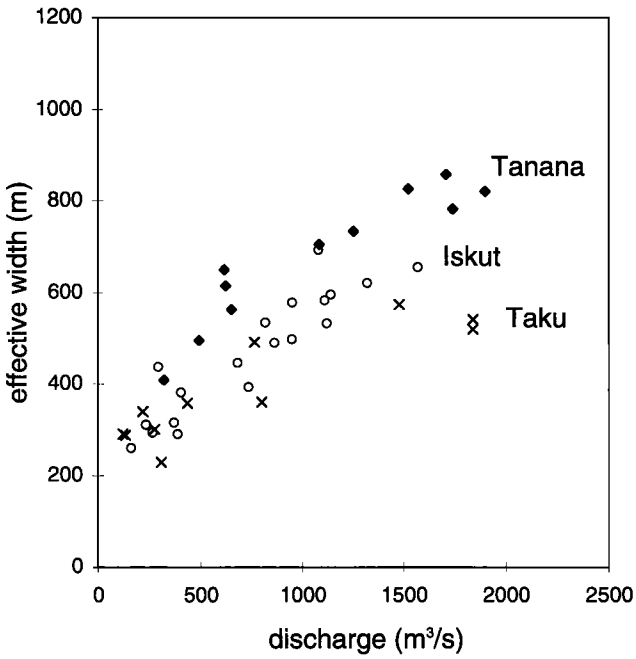

Figure 3. Relationship between satellite-derived effective width W_e and river discharge measured on the ground for the Tanana, Iskut, and Taku Rivers. Each point is determined from a single ERS 1 SAR image and the daily mean discharge measured on the date of image acquisition.

ogy. Three control sections were defined along this transition (T1, T2, and T3 (Figure 4)) to derive effective widths for correlation with ground measurements of discharge (Figure 5). Section T3 is located downstream of the confluence of the Tanana and Chena Rivers. Discharges measured at the Chena River gaging station (18 km upstream of this confluence) were added to the Tanana River discharges for section T3. However, the Chena River inflow was consistently less than 4% of the total flow in the Tanana River, so this correction had a negligible impact on the W_e-Q rating curve derived for section T3.

Because total sinuosity ΣP is a function of discharge, it is problematic to define a single sinuosity index that describes a braided river at all flow conditions. The range of ΣP values for T1, T2, and T3 is 4.43–12.27, 4.82–10.65, and 4.29–5.19, respectively, with median values of 9.6, 6.4, and 4.9. Sinuosities for section T3 are higher than might be expected for a true meandering channel because of the presence of cutoff channels and emergent bars. Figure 5 indicates that the degree of braiding, here approximated by the parameter ΣP, exerts significant control on the relationship between W_e and Q. The sensitivity of water surface area to changing discharge decreases as channel morphology changes from a braided to a nearly meandering configuration. Figure 5 indicates that control sections with high total sinuosities are associated with steeper W_e-Q rating curves. A similar relationship is seen in Figure 3 for the Tanana, Iskut, and Taku Rivers, where median values of ΣP are 9.6, 6.4, and 4.0, respectively. Less scatter is found in the W_e-Q relationships derived from the most intensely braided control sections. Neither the Taku River nor section T3 on the Tanana River is very braided; significant scatter in their W_e-Q rating curves can be seen in Figures 3 and 5.

It should be noted that it is possible for an extremely sinuous meandering channel to have a value of ΣP as large as those from braided channels, yet it will still show little increase in W_e with Q. Other sinuosity or braid indices exist that distinguish meandering from braided channel networks more precisely than the total sinuosity index ΣP used here. However, in the normal spectrum of channel morphologies, values of ΣP are larger for intensely braided rivers than for meandering rivers. The advantage of ΣP is its simple derivation from satellite imagery, without need for consideration of bar dimensions or braid channel orders. From the Tanana, Taku, and Iskut Rivers, as well as the different sites along the Tanana River, the most useful W_e-Q rating curves are associated with large values of ΣP.

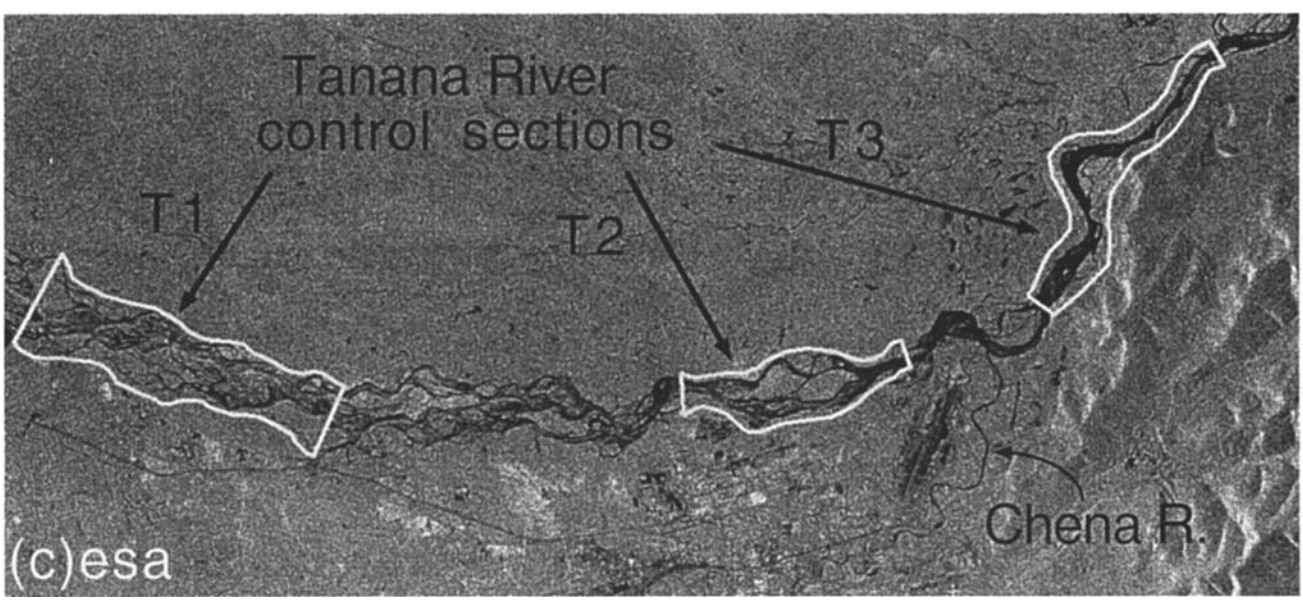

Figure 4. Control sections T1, T2, and T3 from the Tanana River, Alaska, located along a transition from a braided to nearly meandering channel morphology. Satellite-derived W_e-Q rating curves for these three control sections are shown in Figure 5.

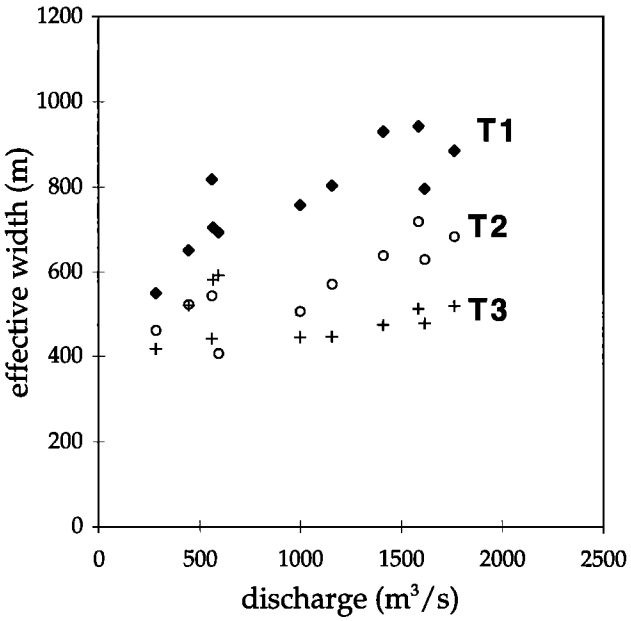

Figure 5. Relationship between satellite-derived effective width W_e and ground measurements of river discharge Q for the Tanana River control sections T1, T2, and T3 in Figure 4. The steepness of the derived W_e-Q rating curve is proportional to the intensity of braiding found in the control section. Median total sinuosities ΣP are 9.6, 6.4, and 4.9 for sections T1, T2, and T3, respectively.

5.3. Monitoring Other River Conditions

Dry and melting river ice, floodplain wetness, and wind conditions can also be interpreted from SAR imagery. As examples, five ERS 1 images acquired over the Tanana River are presented with local meteorological observations from the Fairbanks International Airport in Figure 6. Figure 6b is a typical open-water image, well suited for computation of W_e and ΣP. SAR returns from river ice during midwinter and spring melt conditions are shown in Figures 6d and 6a, respectively. Bright returns from midwinter channel ice surfaces suggest enhanced radar backscattering from an ice-water or ice-slush interface, as *Leconte and Klassen* [1991] observed in airborne SAR images of the Burntwood River, Manitoba. Field measurements of ice thickness carried out on the Tanana River during February and March 1984 by *Lawson et al.* [1986] indicate that the channels do not freeze to the bottom during the winter. Instead, ice thicknesses of 1 m or less were found underlaid by flowing water and pockets of layered frazil ice [*Lawson et al.*, 1986]. If similar conditions existed during the winters of 1992 and 1993, bright areas observed on ERS 1 SAR images of the frozen channel network may correspond to areas of subice water flow or frazil ice accretion.

Strong winds can roughen water surfaces, reducing specular reflection and increasing the backscatter of incident microwaves to the satellite. An extreme example from the Tanana River is shown in Figure 6e. Wind roughening can be a serious problem when using SAR to delineate open water bodies and is discussed further in section 7. Bright returns from the river floodplain in Figure 6c are believed to be backscattered from wet gravel; this is also discussed in section 7.

6. Physical Characterization of the Iskut and Tanana Rivers

As a follow-up to our initial ERS 1 study [*Smith et al.*, 1995], ground measurements of braid channel flow widths, depths, velocities, and water surface slopes were collected from the Iskut River during a field campaign in summer 1994. Similar measurements, as well as sediment grain size distributions, are available for the Tanana River from a series of U.S. Geological Survey reports [*Emmett et al.*, 1978; *Burrows et al.*, 1981; *Burrows and Harrold*, 1983; *Harrold and Burrows*, 1983] and also from R. L. Burrows (U.S. Geological Survey, unpublished field notes, 1977). Limited bed material grain size distributions were collected from the Iskut River as part of a hydroelectric feasibility study [*BC Hydro*, 1981]. The following compilation of these various field data indicates that many of the braid channels from the Tanana River tend to be wider than braid channels from the Iskut River, providing a partial explanation for their differences in the W_e-Q rating curve slope (Figure 3) that is additional to the influence of ΣP already described in section 5.2.

6.1. Braid Channel Hydraulics

Plots of braid channel width versus mean flow depth for the Tanana (47 transects) and Iskut (60 transects) Rivers are shown in Figure 7. Forty of the Iskut River transects were measured from a specially designed river jetboat, using an Impulse QT-206 acoustic depth sounder and an optical rangefinder to estimate braid channel width. Shallow channels were measured with velocity-meter wading rods and a 100-m fiberglass tape. For both rivers, mean depths rarely exceed 2 m despite an extreme range of channel widths (4–165 m for the Iskut; 12–560 m for the Tanana). A unique relationship between braid channel width and discharge does not exist for either river. However, flow width increases roughly with depth, and mean depths tend to center around 1 m. Figure 7 also reveals that over a similar range of mean flow depths the Tanana contains many significantly wider braid channels than does the Iskut.

The hydraulic relationships between channel discharge and width, mean depth, and mean velocity are often expressed in the classical "hydraulic geometry" form of *Leopold and Maddock* [1953]:

$$W = aQ_c^b$$

$$D = cQ_c^d$$

$$V = eQ_c^f$$

where W, D, V, and Q_c are channel width, mean depth, mean velocity, and discharge and a, b, c, d, e, and f are constants. The exponents b, d, and f indicate the sensitivity of channel width, depth, and velocity to changing discharge. As noted by *Ferguson and Ashworth* [1991], these equations express W, D, and V as sole functions of Q_c, an erroneous assumption in some rivers. They also represent a somewhat simplistic view of channel hydraulics and do not explicitly consider any of the complex physical processes that occur at the interface of a moving fluid with a noncohesive bed. A physical understanding of widening in gravel rivers, for example, requires knowledge of the distribution of boundary shear stress, cross-channel sediment transport rates, bank material and angle of repose, and evolution of bed topography [*Pizzuto*, 1990]. Nevertheless,

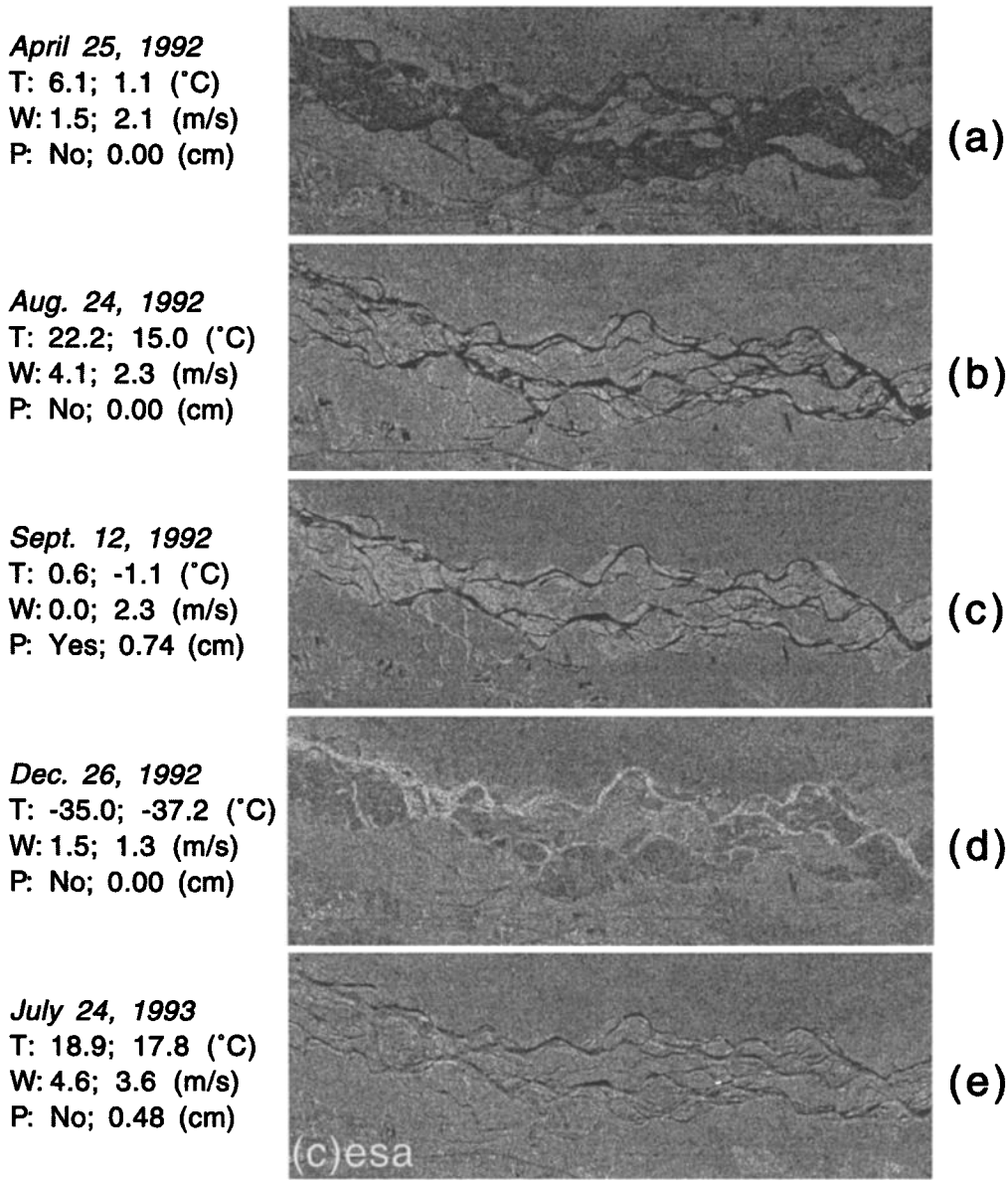

Figure 6. River conditions as interpreted from ERS 1 SAR imagery: (a) melting river ice, (b) typical open water conditions, suitable for calculation of W_e and ΣP, (c) bright returns from bars and islands, interpreted as wet gravel, (d) winter ice, and (e) strong wind conditions, which roughen the water surface, causing increased radar backscattering to the satellite. Each image is 10 × 21 km and is located on the Tanana River near Fairbanks, Alaska. Three-hourly and daily mean weather observations coincident with the times of image acquisition are shown for temperature (degrees Celcius) and wind speed (meters per second). "Yes" or "no" indicates whether precipitation occurred during the 3-hour period associated with the time of image acquisition; precipitation values are daily totals. Weather observations are from Fairbanks International Airport, approximately 15 km distant from the centers of these images.

comparison of the hydraulic geometry exponents among many channels or through time at a station on a single channel permits determination of the relative contribution of flow width, mean depth, and mean velocity to the channel discharge Q_c. Hydraulic measurements from 20 braid channels on the Iskut River yield exponent values $b = 0.51 \pm 0.08$, $d = 0.29 \pm 0.03$, and $f = 0.20 \pm 0.08$ (Figure 8a). Corresponding exponent values from 14 braid channels on the Tanana are $b = 0.65 \pm 0.07$, $d = 0.19 \pm 0.06$, and $f = 0.16 \pm 0.04$ (Figure 8b). The large values of b (relative to values of d and f) indicate that for both rivers, braid channel width increases faster than either mean depth or mean velocity with increasing discharge, a relationship also observed in other braided rivers [*Fahnestock*, 1963; *Church*, 1972; *Rice*, 1979; *Mosley*, 1983]. However, this increase is larger for the Tanana than for the Iskut, as indicated by its larger value of b (Figure 8). This tendency of the Tanana River braid channels to widen, which is also reflected by its large number of very wide channels (Figure 7), provides one physical explanation for its high values of W_e relative to the Iskut River.

Flow velocities in the Iskut were measured on foot, using Price AA current meters at 0.6 flow depth. Water surface slopes were obtained using the method of *Laperriere and Martin* [1986], using a flexible, water-filled clear plastic tube to

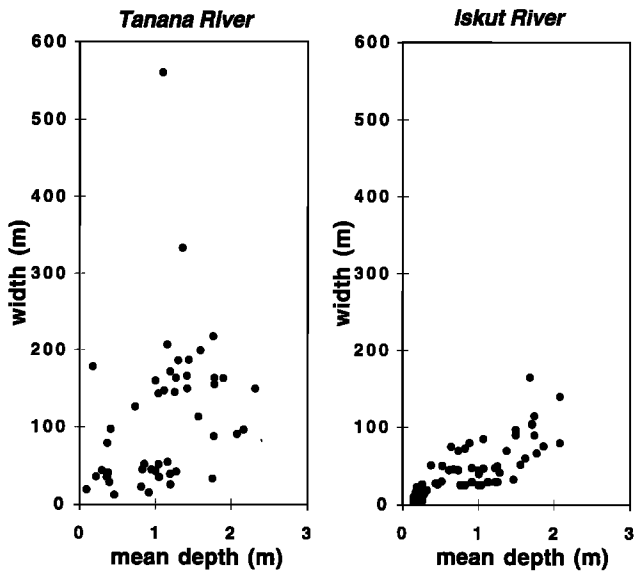

Figure 7. Field measurements of braid channel width versus mean depth for the Tanana and Iskut Rivers. While no unique relationship exists between width and mean depth, depths cluster around 1 m, and the range of widths is greatest for the Tanana River.

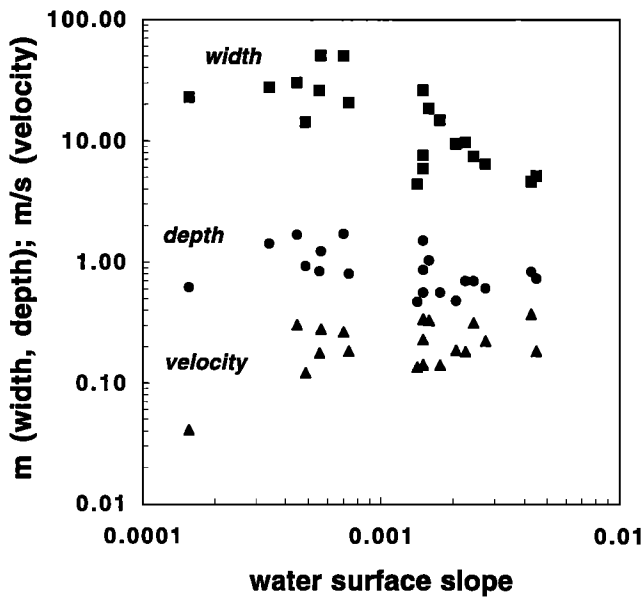

Figure 9. Field measurements of water surface slope versus channel width, mean depth, and mean velocity from 20 braid channels on the Iskut River. Width is the most sensitive hydraulic variable to changes in water surface slope, and gentler slopes are associated with wider braid channels.

measure relative water surface elevation differences 10 m apart. The relationship between slope and channel width, mean depth, and mean velocity for 20 braid channels is shown in Figure 9. Despite significant scatter in the data, channel width appears to be more sensitive than depth or velocity to slope, although small increases in velocity and decreases in depth do occur as water surface slopes become greater. Steeper slopes are associated with narrower channels, while gentler slopes are associated with wider channels. A similar relationship may exist at the floodplain scale: The Tanana River possesses a gentler valley slope and wider braid channels than does the Iskut River. Knowledge of valley slope may be required for parameterization of satellite-derived W_e-Q rating curves, which may reflect a river's propensity for braid channel widening.

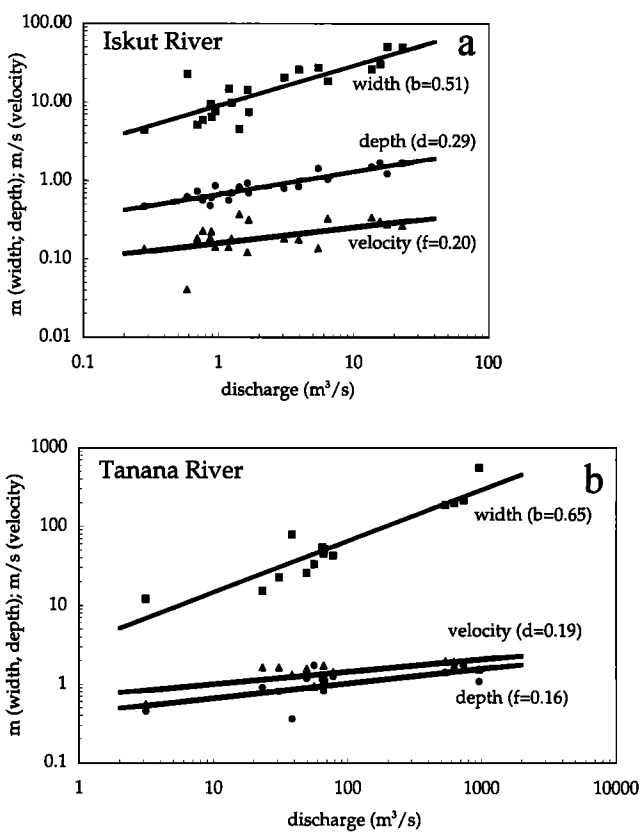

Figure 8. Field measurements of braid channel width, depth, and mean velocity versus braid channel discharge for (a) the Iskut and (b) Tanana Rivers.

6.2. Valley Slope and Grain Size

The Iskut River drains a heavily glacierized basin and flows with a moderate gradient over a coarse gravel bed. The Tanana River near Fairbanks, Alaska, is 150 km distant from its glacial sources, has a gentle slope, and flows over silt, sand, and gravel. Valley gradients derived from topographic maps for the Tanana and Iskut Rivers control sections are 0.0010 and 0.0022, respectively. Bed material grain size distributions have previously been measured for the Tanana River [*Harrold and Burrows*, 1983] and, to a limited extent, for the Iskut River [*BC Hydro*, 1981] (Figure 10). Average median grain sizes (d_{50}) from three transects on the Iskut were 10.0, 16.1, and 17.2 mm, yielding a mean value of 14.4 mm. Average median grain sizes from 10 transects on the Tanana River in 1981 ranged from 0.21 to 22 mm [*Burrows and Harrold*, 1983], with a mean value of 9.9 mm.

Previously measured grain size distributions from the Taku River control section were not available. Although *Slatt and Hoskin* [1968] noted that the Taku River sediments approximately 50 km downstream of the control section are composed predominantly of gravel, this likely results from inputs of coarse sediment from several glaciers between their site and the control section used in this study. The low valley gradient (0.0015) and presence of a large marsh near the Taku River

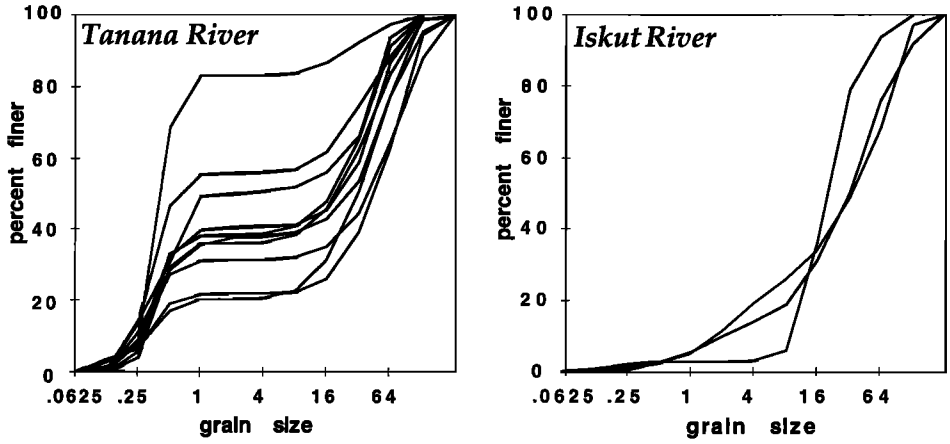

Figure 10. Cumulative bed surface material grain size distributions from the Tanana and Iskut Rivers. The Iskut is composed predominantly of gravel; the Tanana also contains a high proportion of sand and silt.

control section suggest that fine sediments are present in the bed material of the study reach, but without field observations, no assumptions about size distribution can be made.

7. Problems and Errors

7.1. Sensor Resolution and Incidence Angle

Oblique air photos of the Iskut River taken within hours of two ERS 1 data acquisitions show that the 25-m nominal spatial resolution of ERS 1 cannot always resolve small braid channels of about 10 m in width, limiting application of this technique to large braided rivers (with flows of the order of 1000 m^3/s) when using ERS data. This resolution limitation causes a small but uncertain underestimation in the measurement of total water surface area. Errors consequently introduced to the discharge estimate are likely to be small: Inspection of Figure 7 shows that for large braided systems such as the Tanana and Iskut Rivers much of the flow is accommodated by wider channels. Also, discharge per unit width is greatest in wide, deep braid channels, which normally experience less frictional resistance throughout their velocity profiles than do smaller channels. As described earlier in section 4.2, failure to resolve small channels adequately also introduces error to the computation of ΣP. For areas where cloud cover is not a problem, high-resolution visible/near-infrared sensors such as the forthcoming advanced spaceborne thermal emission and reflection radiometer (ASTER) or the currently operating Système Probatoire d'Observation de la Terre (SPOT) (10 m panchromatic) should provide estimates of W_e that are more precise than those obtained from ERS SAR imagery. Successful application of this technique to rivers smaller than the three studied here is probably not possible with ERS 1 or 2. However, the new RADARSAT will provide SAR data of 9-m spatial resolution when in high-resolution mode. This represents a significant increase in spatial resolution that may permit discharge estimates to be made for smaller braided streams.

Specular returns from open water surfaces may be enhanced with increased sensor incidence angle. The space shuttle *Endeavor* acquired a SIR-C SAR scene over More Creek, a braided tributary to the Iskut River, in April 1994. Comparison with ERS 1 images acquired over the same area shows that water surfaces can be seen more distinctly in the SIR-C data, despite the similar spatial resolutions of the two sensors. This is likely due to the greater sensor incidence angle (36° versus 24° for ERS 1) used during the SIR-C mission. Foreshortening and layover, topographic distortions commonly found in SAR data acquired over rugged terrain, are also less severe in the SIR-C data, although radar shadow effects are increased. Returns from braided river floodplains are sometimes masked by layover effects from the surrounding topography. The pointing capability of RADARSAT permits different sensor incidence angles to be used during data acquisition. Choice of a high angle, such as that used during the SIR-C missions, may improve the ability of the SAR to discriminate small braid channels and also reduce topographic layover effects onto the river floodplain.

7.2. Wind

Strong winds induce waves on open water surfaces, reducing specular reflection and increasing the amount of incident energy backscattered to the satellite. This is a common phenomenon on lakes and wide, calm rivers but occurred infrequently on the braided rivers studied here. Wind was an occasional problem for the Tanana River but not for the Iskut or Taku. Nevertheless, it can make discrimination of the water surface difficult or impossible, as shown for the Tanana River in Figure 6e. From ERS 1 images and 3-hour averages of wind speed recorded at the Fairbanks International Airport, wind roughening can become problematic above wind speeds of 4 m/s; however, conditions at the exact moment of image acquisition are unknown. Wind roughening is spatially discontinuous and becomes more common as flow widths increase and flow velocities decrease.

7.3. Wet Gravel Bars

Unusually high backscatter values from bars surrounding and among the braid channels were observed in five ERS 1 images acquired over the Tanana River (Figure 6c). Streamflow and local meteorological records suggest that these strong returns were caused by wet gravel conditions. Two of the five anomalous images were associated with rainfall, one was associated with snowfall at temperatures slightly above freezing, and two were associated with sharply falling river stage. Strong, bright returns from these areas can actually "overwhelm" small channels and cause larger channels to appear narrow to the

Table 2. Values of Discharge Q and Effective Width W_e Generated From a Cellular Automata Model of Stream Braiding

Q, m^3/s	W_e
12	7.5
18	10.7
24	14.8
30	15.8
36	18.9
42	23.4
48	21.6
54	24.3
60	26.6
66	27.1
72	29.8

Q is varied by increasing the number of cells receiving discharge in the first row of the model lattice. For each model run, time-averaged values of W_e were obtained from the downstream half of the lattice after an apparent statistical steady state was reached.

water classification algorithm. For the Tanana River the presence of more than 4% area of wet gravel caused a significant underestimation in water surface area; such scenes were discarded.

7.4. Other Errors

Three other errors are known to effect the presented methodology: First, all radiometric and geometric corrections applied to each ERS 1 image are applied to the Goddard Earth Model (06) geoid model. Surface elevation and departures of the true geoid from this model are not considered, producing small but uncertain errors in mountainous regions. Second, control sections must be located manually, as ERS 1 image location errors are of the order of 200 m [*Bicknell*, 1992]. Human-induced inconsistency in locating control sections was determined to cause errors in the calculated water surface area ranging from 0.1 to 13%, with an average error of under 3%. Last, ground discharge data used to calibrate the W_e-Q rating curves presented here are of variable quality. The U.S. Geological Survey streamflow records are rated poor to good (Tanana River) and fair to good (Taku River). Tanana River data were corrected for additional flow through Salchaket Slough, which bypasses the gaging station. This correction increases discharge measurements at the Fairbanks gaging station by around 9% and is based on simultaneous ground discharge measurements from both sites (R. L. Burrows, U.S. Geological Survey, unpublished field notes, 1973–1975). The Water Survey of Canada's discharge record for the Iskut River is not rated but contains many estimated values, and stage-discharge rating curves have been reconstructed frequently, suggesting a relatively unstable channel cross section at the gaging station.

8. W_e-Q Relationship From a Cellular Model of Stream Braiding

A simple computer model of stream braiding [*Murray and Paola*, 1994] was used to generate values of effective width associated with different steady state discharges. The model is similar to the cellular automata models developed in dynamical systems research and is of the type called a coupled map lattice by *Kaneko* [1993]. The model produces qualitatively realistic behavior [*Murray and Paola*, 1994], and the generated spatial patterns exhibit many of the same features as real rivers [*Murray and Paola*, 1996a].

Initial prerun bed topography has an overall slope containing random perturbations. At the beginning of a run, discharge is introduced to some cells at the upstream end of the lattice. A simple uniform flow approximation rule routes the discharge from each cell to its immediate downstream neighbors by an amount determined from the local bed topography. Sediment is transported from a cell into a downstream neighbor cell according to the rule

$$Q_s = K[QS + 0.35^* \sum (Q_{ut}S_{ut})]^{2.5}$$

where Q_s is the amount of sediment transferred, Q is the cell discharge, S is the slope to the downstream neighbor cell, Q_{ut} and S_{ut} are discharge and slope from the upstream immediate neighbor cells, and K is a constant. The product QS is the local stream power index, and the exponent of 2.5 comes from empirical whole-river studies relating sediment transport to stream power [*Ashmore*, 1985]. An additional flow momentum term (0.35) permits sediment transport over locally flat or uphill slopes, as occurs in real rivers. An additional rule transfers a small amount of sediment down lateral slopes adjacent to a cell containing discharge. The rule is consistent with semiempirical equations for the component of sediment transport induced directly by gravity. Each iteration ends when discharge reaches the downstream end of the lattice. The elevation of each cell is adjusted according to the difference between the amount of sediment entering and leaving that cell (a discretization of the Exner equation). Boundary conditions consist of high side walls to contain the flow. Cell elevations in the first and last rows remain fixed.

The model has no fixed spatial scale, and grain size is not considered. The model is designed to represent large-scale interactions. For example, lattice cells are assumed to be large relative to flow depth in order for uniform flow to be a good approximation. However, the absolute size of the cells is not constrained. A given simulation could represent a laboratory-scale stream or a field-scale river; the cell dimensions can be arbitrarily chosen [*Murray and Paola*, 1996a, b]. Similarly, other quantities in the model are given in arbitrary units. For instance, we introduce 25,000 arbitrary discharge units into each of the cells in the first row that receive discharge. This number could represent 1 dL/s if we choose a laboratory-scale stream as the prototype for the model, or it could represent 100 L/s if we choose a field-scale river. Changing the number of arbitrary discharge units changes the amount of sediment transport in each cell by the same amount; the model merely develops at a different rate. This ambiguity in comparing the units in the model to those in a real river does not present a problem for the present purpose, which is to explore how the effective width of a simple braided-stream model varies with the discharge, independent of scale.

In the simulations reported here, discharge is varied by changing the number of cells in the first row that receive discharge. Table 2 lists the number of cells in the first row receiving discharge for 11 simulations, using a braid plain that is 72 cells wide and 500 cells long. Model effective width is the average number of cells in a cross section that contain a discharge greater than an arbitrary cutoff, which is 8000 discharge units for these simulations (approximately 2% of the total discharge in the narrowest run). Once the model has reached an apparent statistical steady state, the effective widths at five different times are averaged to produce the values in Table 2.

Effective widths were sampled only in the downstream half of the braidplain to avoid "introduction effects," such as channel entrenchment near the upstream lattice boundary [*Murray and Paola*, 1996a, b].

The correlation between model-generated discharge and effective width is shown in Figure 11 (values of Q and W_e have been normalized to 1.0). A smooth, power law relationship similar to the satellite-derived curves for the Tanana, Iskut, and Taku Rivers (Figure 3) is found, providing theoretical support for fitting power law curves to the limited data on real rivers derived from ERS 1 images and ground discharge measurements. However, the best fit exponent of this power function is 0.75, which is considerably larger than exponents for the three natural rivers presented in Figure 3. This is an expected consequence of the model's assumption of a perfectly noncohesive channel bed and is discussed further in section 9.1.

This model is not completely realistic; it excludes many of the small-scale processes that occur in real braided rivers. However, Figure 11 shows that even a simple cellular model of stream braiding shows a smooth and nonlinear correlation between effective width and discharge. A linear increase would imply that the maximum local (per unit width) discharge that could be produced within the system is independent of the total discharge. The observed nonlinearity suggests that this is not the case. Instead, higher total discharges create the possibility of greater maximum flows in confluences and hence higher maximum local discharges, without need for a linear increase in active flow area.

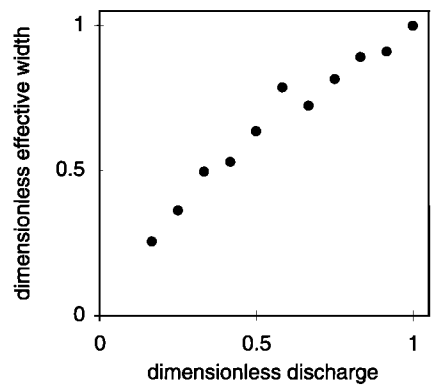

Figure 11. Relationship between values of effective width W_e and discharge Q from a cellular model of stream braiding. Units are dimensionless; the largest generated values of W_e and Q have been normalized to 1.0.

9. Discussion

9.1. Potential for Application to Ungaged Basins

The satellite-derived rating curves which relate effective width W_e to river discharge Q in Figure 3 indicate that the active flow area on braided rivers is strongly correlated with discharge. For rivers where satellite imagery and ground streamflow measurements are available this relationship can be empirically determined and used to obtain estimates of instantaneous river discharge from space. For the three study rivers, differences between predicted and actual discharge ranged from 6 to 633 m^3/s. Values of W_e from satellite imagery display a smooth power law correlation with ground measurements of discharge. Synthetic values of W_e and Q generated from a cellular model of stream braiding also show a smooth power law correlation, despite the relative simplicity of the model. This provides some theoretical support for the observation that flow area increases smoothly and nonlinearly with discharge and suggests that it is appropriate to fit power functions through empirically derived plots of W_e and Q. However, the width exponent of the modeled W_e-Q rating curve is significantly larger (0.75) than all of the empirically derived curves presented here. A likely reason for this is that the model assumes a perfectly noncohesive channel bed. Also, stabilization from vegetation is not considered. All of the rivers examined in this study contain trees and shrubs on some bars, which contribute significantly to bank stability. This difference may explain why effective widths vary less with discharge in these natural systems than in the cellular model: Stabilization generally makes banks steeper and also reduces the braid channel's ability to widen with increasing discharge.

For rivers where ground streamflow measurements are not available, relative changes in discharge can be observed from space using this method. Determination of absolute discharge poses a more difficult problem. From the data presented here for the Tanana, Iskut, and Taku Rivers a single best fit W_e-Q rating curve of the form $W_e = 38Q^{0.39}$ may be calculated. Indiscriminate use of this function for the three rivers studied here would produce large errors; however, as an approximation, it would seem possible to estimate absolute discharge within a factor of 2. Errors would be significantly reduced by collecting one or more field measurements of streamflow simultaneously with a satellite overpass, particularly if obtained during high-flow conditions. It should be noted that the Tanana and Taku Rivers, which possess the steepest and flattest W_e-Q rating curves in Figure 3, respectively, may represent morphological end members in the braided river spectrum. The Tanana possesses the second gentlest valley gradient out of 55 braided rivers in Alaska and northwest Canada (locations shown in Figure 1), while the Taku is not very braided (ΣP values range from 1.98 to 6.33 over a flow range of 124 to 1840 m^3/s). However, the Iskut and Taku Rivers also have relatively gentle valley gradients. W_e-Q rating curves must be constructed for some steeper braided rivers before any generalized empirical rating curve can be proposed.

An alternative approach is to seek ways to parameterize the satellite-derived rating curves presented in Figure 3, using morphologic and hydraulic channel characteristics. When compared to the full spectrum of possible alluvial river channel morphologies, all braided rivers share some gross similarities. There is also some evidence that the relationship between braid channel width and discharge can be similar among rivers of like geographic location: *Mosley* [1983] found nearly identical width exponents for three braided rivers in New Zealand, with b values of 0.35, 0.36, and 0.32 [*Mosley*, 1983]. However, total sinuosity, valley gradient, sediment supply and size distribution, bank stability, vegetation cover type and extent, and range of discharge fluctuations all influence the relationship between water surface area and discharge. If knowledge of all of these factors is prerequisite for effective parameterization of a generalized W_e-Q rating curve, the prospect of using satellites to measure discharge in remote rivers loses a considerable amount of its appeal. However, our examination of the total sinuosity parameter ΣP indicates that it is a major contributor to differences in W_e-Q rating-curve slope: The sensitivity of water surface area as a measure of total discharge is highly dependent upon the degree of braiding. This dependency is

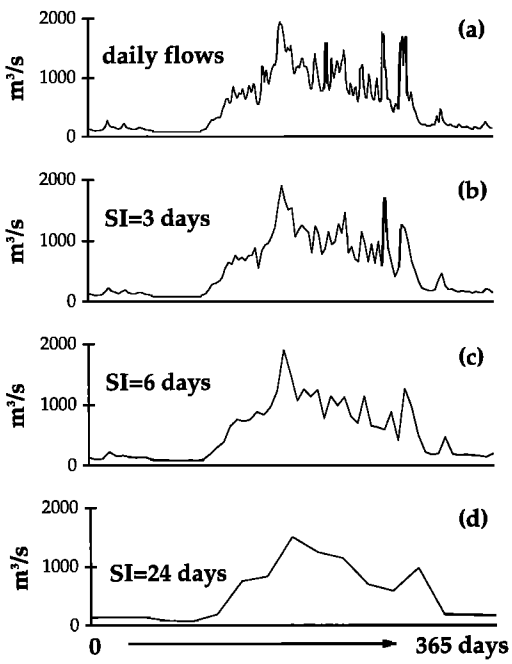

Figure 12. Subsampling of a 1-year daily discharge record from the Iskut River, with sample intervals (SI) of 3, 6, and 24 days. Such watersheds are dominated by the melting of ice and snow, producing a high-flow period lasting several months. Although brief flood events are quickly lost with increasing SI, the overall timing and volume of the annual hydrograph are preserved and may be resolved using intermittent satellite-derived discharge estimates.

found among the Tanana, Taku, and Iskut Rivers, as well as for three different sites along the Tanana River. Comparison of the range of ΣP values computed for the Tanana, Iskut, and Taku Rivers (Table 2) indicates that low total sinuosities are associated with a flatter W_e-Q rating curve (e.g., the Taku River), while high sinuosities correspond to a more sensitive rating curve (e.g., the Tanana River). Total sinuosity is a useful parameter because it may be obtained from satellite images or air photos. It is also dependent upon many of the morphological variables described earlier. Its greatest drawback is its strong dependency on discharge, which makes determination of a single value of ΣP for a particular river rather meaningless.

Our findings indicate that the nominal 25-m spatial resolution of ERS SAR imagery is not sufficient for revealing any differences in the relationship between W_e and ΣP among the Tanana, Iskut, and Taku Rivers. It is likely that such differences do exist among braided rivers of differing vegetation cover, sediment supply and size distribution, and valley slope. For example, braided rivers containing vegetated islands or more cohesive bank material may experience a more rapid increase in W_e (relative to ΣP) with increasing discharge than very sandy, nonvegetated systems, if existing channels widen faster than new ones form. In principle, even though W_e and ΣP will increase with discharge for both rivers, differences in their rates of increase could be used to constrain selection of an appropriate W_e-Q rating curve for application to ungaged sites, based on previously compiled rating curves relating discharge as a function of both W_e and ΣP.

Comparison of braid channel widths, valley slope, and bed material grain size distributions for the Iskut and Tanana Rivers suggests that these morphological constraints do influence the shape of the W_e-Q relationship, but they undoubtedly relate to total sinuosity as well. The Tanana River has the highest effective widths of the three rivers. Field measurements indicate that it has a gentler valley gradient, finer bed-material grain size, and wider braid channels than the Iskut River. ERS 1 SAR images show that it also has larger values of ΣP. However, it is uncertain if total sinuosity alone is enough to parameterize a generalized W_e-Q rating curve for application to ungaged basins. Instead, a combination of parameters, such as total sinuosity, valley slope, the distribution of braid channel widths, and vegetation cover will likely be needed before discharge may be accurately estimated from ungaged sites without any calibrating ground measurements of discharge.

9.2. Sampling Frequency

Until high-resolution satellite data are consistently acquired at least once every 2–3 days, implementation of a space-based streamflow monitoring program will be of limited utility for detecting brief flood events. However, seasonal streamflow cycles in glacierized basins (where rivers are commonly braided) are strongly correlated with mean temperature, producing flows that swell over a period of weeks to months. The contribution of stochastic rainfall events to total annual flow is commonly minor when compared with the volume of water produced by the melting of ice and snow. As a result, intermittent discharge measurements may be adequate for approximating the timing and volume of the annual hydrograph in glacierized basins. For illustration, 1 year of daily ground measurements of discharge from the glacierized Iskut River is shown in Figure 12a. The record is subsampled using time intervals of 3, 6, and 24 days as examples of satellite data acquisition frequencies (Figures 12b, 12c, and 12d). As the length of time between measurements is increased, short-duration flow events are lost, but the overall shape and volume of the annual hydrograph are preserved. For the purpose of determining the shape of the annual hydrograph, satellite return intervals of about 1 week should be sufficient for alpine or high-latitude watersheds where flows are dominated by melt processes. Current high-resolution satellite return times are of the order of days to weeks and are improving rapidly with the advent of additional SAR sensors such as ERS 2, RADARSAT, and ENVISAT 1, a next generation SAR scheduled for launch by the European Space Agency in 1998.

10. Conclusions

Forty-one ERS 1 SAR images and simultaneous ground measurements of discharge for three large braided rivers were used to show that the area of active flow on braided river floodplains is primarily a function of discharge. Plots of satellite-derived effective width W_e versus discharge Q suggest a smooth power law relationship between W_e and Q. Synthetic values of W_e and Q generated by a cellular model of stream braiding also show a smooth power law correlation. For rivers where gaging station data are available to ascertain the W_e-Q relationship, discharge can subsequently be estimated from satellite data alone with errors ranging from tens to hundreds of cubic meters per second if ERS SAR data are used.

For ungaged rivers the shape of the annual hydrograph can be established using high-resolution satellite imagery to estimate relative discharge. Absolute discharge can probably be estimated within a factor of 2, with more accurate values re-

quiring either (1) one or more ground measurements of streamflow acquired simultaneously with a satellite image acquisition, or (2) successful parameterization of morphologic controls such as total sinuosity ΣP, slope, vegetation cover, and distribution of braid channel widths. Our comparison of ΣP values computed from satellite imagery, valley gradients measured from topographic maps, and field hydraulic measurements collected at two rivers indicates that while such parameterization is complex and will require consideration of several morphologic and sedimentologic variables, total sinuosity exerts the most significant control upon satellite-derived W_e-Q rating curves. Selection of large, intensely braided control sections 10 km or more in length will yield best results when using this satellite-based technique to estimate discharge in braided rivers.

Acknowledgments. Support for this work was provided by NASA through Earth Observing System (EOS) grant NAGW-2638, Spaceborne Imaging Radar (SIR-C) grant 958745, and a Graduate Student Researchers Program Fellowship NGT-51223. Modeling efforts were supported by the National Science Foundation (DMS 93-16078 and EAR 94-05807). ERS 1 data were provided by the European Space Agency and acquired by the Alaska SAR Facility. Ground measurements of river discharge were collected by the Water Survey of Canada and the U.S. Geological Survey WRD; the latter also donated field equipment for use on the Iskut River. Support for the field campaign was supplemented by the Geological Society of America and a Sage Graduate (Cornell University) summer research grant. River and air transport in British Columbia was provided by Cominco Snip Operation, Pamicon Inc., TH Charters, Northern Mountain Helicopter, and Sunrise Aviation. Assistance from T. Blodgett, A. Krat, J. Liebeskind, I. Preuss, and C. Shopis of Cornell University is gratefully acknowledged. Helpful comments were made by two anonymous reviewers, Chris Paola (University of Minnesota), and R. L. Burrows (USGS-WRD, Fairbanks), who also provided unpublished field data for the Tanana River. INSTOC contribution 226.

References

Allison, L. J., T. J. Schmugge, and G. Byrne, A hydrologic analysis of east Australian floods using Nimbus-5 electrically scanning radiometer data, *Bull. Am. Meteorol. Soc.*, *60*, 1414–1427, 1979.

Ashmore, P. E., Process and form in gravel braided streams: Laboratory modelling and field observations, Ph.D. thesis, Univ. of Alberta, Edmonton, Canada, 1985.

Barton, I. J., and J. M. Bathols, Monitoring floods with AVHRR, *Remote Sens. Environ.*, *30*, 89–94, 1989.

BC Hydro, Hydroelectric Generation Projects Division, Stikine-Iskut hydroelectric development feasibility study: Hydrology, river regime, and morphology, *Rep. H-1110*, Vancouver, B. C., Canada, 1981.

Berg, C. P., D. R. Wiesnet, and M. Matson, Assessing the Red River of the North 1978 flooding from NOAA satellite data, in *Satellite Hydrology, Proceedings of the Fifth Annual William T. Pecora Memorial Symposium on Remote Sensing, Tech. Publ. Ser. TPS81-1*, pp. 309–315, Am. Water Resour. Assoc., Bethesda, Md., 1981.

Bicknell, T., User's guide to products: Version 1.0., *Rep. JPL D-9362*, 11 pp., Jet Propul. Lab., Pasadena, Calif., 1992.

Blasco, F., M. F. Bellan, and M. U. Chaudhury, Estimating the extent of floods in Bangladesh using SPOT data, *Remote Sens. Environ.*, *39*, 167–178, 1992.

Blyth, K., and D. S. Biggin, Monitoring floodwater inundation with ERS 1 SAR, *Earth Obs. Q.*, *42*, 6–8, 1993.

Brakenridge, G. R., J. C. Knox, E. D. Paylor, and F. J. Magilligan, Radar remote sensing aids study of the great flood of 1993, *Eos Trans. AGU*, *75*(45), 521–527, 1994.

Brooner, W. G., and C. M. V. Binaghi, Landsat monitoring of temporal hydrological variations on the Pilcomayo River, 1972–1981, paper presented at Seventeenth International Symposium on Remote Sensing of the Environment, Univ. of Mich., Ann Arbor, 1983.

Burrows, R. L., and P. E. Harrold, Sediment transport in the Tanana River near Fairbanks, Alaska, 1980–81, *U.S. Geol. Surv. Water Resour. Invest.*, *83-4064*, 116 pp., 1983.

Burrows, R. L., W. W. Emmett, and B. Parks, Sediment transport in the Tanana River near Fairbanks, Alaska, 1977–1979, *U.S. Geol. Surv. Water Resour. Invest.*, *81-20*, 62 pp., 1981.

Chalah, C., T. Korme, J. Chorowcz, C. Mering, and J. P. Rudant, Remote sensing for agriculture, forestry, and natural resources, *Proc. SPIE Int. Soc. Opt. Eng.*, *2585*, 178–188, 1995.

Choudhury, B. J., Passive microwave remote sensing contribution to hydrological variables, *Surv. Geophys.*, *12*, 63–84, 1991.

Church, M., Baffin island sandurs: A study of Arctic processes, *Bull. Geol. Surv. Can.*, *216*, 208 pp., 1972.

Emmett, W. W., R. L. Burrows, and B. Parks, Sediment transport in the Tanana River in the vicinity of Fairbanks, Alaska, 1977, *U.S. Geol. Surv. Open File Rep.*, *78-290*, 28 pp., 1978.

Fahnestock, R. K., Morphology and hydrology of a glacial stream: White River, Mount Rainier, Washington, *U.S. Geol. Surv. Prof. Pap.*, *422-A*, 70 pp., 1963.

Ferguson, R., and P. Ashworth, Slope-induced changes in channel character along a gravel-bed stream: The Allt Dubhaig, Scotland, *Earth Surf. Processes Landforms*, *16*, 65–82, 1991.

Gupta, R. P., and S. Banerji, Monitoring of reservoir volume using Landsat data, *J. Hydrol.*, *77*, 159–170, 1985.

Haeberli, W., P. Müller, P. Alean, and H. Bösch, Glacier changes following the Little Ice Age—A survey of the international data basis and its perspectives, in *Glacier Fluctuations and Climatic Change*, edited by J. Oerlemans, pp. 77–101, Kluwer Acad., Norwell, Mass., 1989.

Halberg, G. R., B. E. Hoyer, and A. Rango, Application of ERTS-1 imagery to flood inundation mapping, in *Symposium on Significant Results From the Earth Resources Technology Satellite-1*, vol. 1, *Technical Presentations, Section A*, *NASA Spec. Publ.*, *327*, 745–753, 1973.

Hamilton, S. K., S. J. Sippel, and J. M. Melack, Inundation patterns in the Pantanal wetland of South America determined from passive microwave remote sensing, *Arch. Hydrobiol.*, in press, 1996.

Harrold, P. E., and R. L. Burrows, Sediment transport in the Tanana River near Fairbanks, Alaska, 1982, *U.S. Geol. Surv. Water Resour. Invest.*, *83-4213*, 53 pp., 1983.

Hess, L. L., and J. M. Melack, Mapping wetland hydrology and vegetation with synthetic aperture radar, *Int. J. Ecol. Environ. Sci.*, *20*, 197–205, 1994.

Hess, L. L., J. M. Melack, and D. S. Simonett, Radar detection of flooding beneath the forest canopy: A review, *Int. J. Remote Sens.*, *11*(7), 1313–1325, 1990.

Hess, L. L., J. M. Melack, S. Filoso, and Y. Wang, Delineation of inundated area and vegetation along the Amazon floodplain with the SIR-C synthetic aperture radar, *IEEE Trans. Geosci. Remote Sens.*, *33*(4), 896–904, 1995.

Hockey, B., T. Richards, and H. Osmaston, Prospects for operational remote sensing of surface water, *Remote Sens. Rev.*, *4*(2), 265–283, 1990.

Hong, L. B., and T. R. H. Davies, A study of stream braiding, *Geol. Soc. Am. Bull.*, *Part 1*, *82*, 1251–1266, 1979.

Imhoff, M. L., C. Vermillion, M. H. Story, A. M. Choudhury, A. Gafoor, and F. Polcyn, Monsoon flood boundary delineation and damage assessment using space borne imaging radar and Landsat data, *Photogramm. Eng. Remote Sens.*, *53*(4), 405–413, 1987.

Kaneko, K., *Theory and Applications of Coupled Map Lattices*, 189 pp., John Wiley, New York, 1993.

Kannen, A., Use of SAR data for flood mapping and monitoring in Thuringia, Germany, paper presented at First Thematic Working Group Meeting on Flood Monitoring, ESRIN/Eur. Space Agency, Frascati, Italy, June 26–27, 1995.

Kellndorfer, J., T. Schadt, and W. Mauser, Segmented land use classification of multitemporal ERS-1 SAR data using a majority filter, in *Proceedings of the First ERS-1 Symposium, Eur. Space Agency Spec. Publ., ESA-SP-359*, 523–526, 1993.

Koblinsky, C. J., R. T. Clarke, A. C. Brenner, and H. Frey, Measurement of river level variations with satellite altimetry, *Water Resour. Res.*, *29*(6), 1839–1848, 1993.

Kruus, J., M. Deutsch, P. L. Hansen, and H. L. Ferguson, Flood applications of satellite imagery, in *Satellite Hydrology, Proceedings of the Fifth Annual William T. Pecora Memorial Symposium on Remote Sensing, Tech. Publ. Ser. TPS81-1*, pp. 292–301, Am. Water Resour. Assoc., Bethesda, Md., 1981.

Laperriere, J. D., and D. C. Martin, Simplified method of measuring stream slope, in *Proceedings of the Symposium on Cold Regions*

Hydrology, edited by D. L. Kane, *Tech. Publ. Ser. TPS-86-1*, pp. 143–145, Am. Water Resour. Assoc., Bethesda, Md., 1986.

Lawson, D. E., D. F. Chacho, B. E. Brockett, J. L. Wuebben, C. M. Collins, S. A. Arcone, and A. J. Delaney, Morphology, hydraulics, and sediment transport of an ice-covered river: Field techniques and initial data, *CRREL Rep. 86-11*, 37 pp., Cold Reg. Res. and Eng. Lab., Hanover, N. H., 1986.

Leconte, R., and P. D. Klassen, Lake and river ice investigations in northern Manitoba using airborne SAR imagery, *Arctic*, *44*, suppl. 1, 153–163, 1991.

Leopold, L. B., and T. Maddock, The hydraulic geometry of stream channels and some physiographic implications, *U.S. Geol. Surv. Prof. Pap.*, *252*, 57 pp., 1953.

Manabe, S., and R. T. Wetherald, On the distribution of climate change resulting from an increase in CO_2 content of the atmosphere, *J. Atmos. Sci.*, *39*, 99–118, 1980.

Manabe, S., R. J. Stouffer, M. Spelman, and K. Bryan, Transient responses of coupled ocean-atmosphere model to gradual changes of atmospheric CO_2, I, Annual mean response, *J. Clim.*, *4*, 785–818, 1991.

Meier, M. F., Contribution of small glaciers to global sea level, *Science*, *226*, 1418–1421, 1984.

Melack, J. M., L. L. Hess, and S. Sippel, Remote sensing of lakes and floodplains in the Amazon Basin, *Remote Sens. Rev.*, *10*, 127–142, 1994.

Mitchell, J., T. Johns, J. Gregory, and S. Tett, Climate response to increasing levels of greenhouse gases and sulphate aerosols, *Nature*, *376*, 501–504, 1995.

Morrison, R. B., and P. G. White, Monitoring flood inundation, in *ERTS-1: A New Window on Our Planet*, *U.S. Geol. Surv. Prof. Pap.*, *929*, 196–208, 1976.

Mosley, M. P., Response of braided rivers to changing discharge, *J. Hydrol. N.Z.*, *22*(1), 18–67, 1983.

Murray, A. B., and C. Paola, A cellular model of braided rivers, *Nature*, *371*, 54–57, 1994.

Murray, A. B., and C. Paola, A new quantitative test of geomorphic models, applied to a model of braided streams, *Water Resour. Res.*, in press, 1996a.

Murray, A. B., and C. Paola, Properties of a cellular braided stream model, *Earth Surf. Processes*, in press, 1996b.

Noyelle, J., S. Delmeire, and L. Marinelli, Identification of flooded areas in the Rhone and Var rivers, France, using ERS-1 data, paper presented at First Thematic Working Group Meeting on Flood Monitoring, ESRIN/Eur. Space Agency, Frascati, Italy, June 26–27, 1995.

Ormsby, J. P., B. J. Blanchard, and A. J. Blanchard, Detection of lowland flooding using active microwave systems, *Photogramm. Eng. Remote Sens.*, *51*, 317–328, 1985.

Pizzuto, J. E., Numerical simulation of gravel river widening, *Water Resour. Res.*, *26*(9), 1971–1980, 1990.

Pope, K. O., E. J. Sheffner, K. J. Linthicum, C. L. Bailey, T. M. Logan, E. S. Kasischke, K. Birney, A. R. Njogu, and C. R. Roberts, Identification of central Kenyan Rift Valley fever virus vector habits with Landsat TM and evaluation of their flooding status with airborne imaging radar, *Remote Sens. Environ.*, *40*, 185–196, 1992.

Rango, A., and A. T. Anderson, Flood hazard studies in the Mississippi River basin using remote sensing, *Water Resour. Bull.*, *10*(5), 1060–1081, 1974.

Rice, R. J., The hydraulic geometry of the lower portion of the Sunwapta River valley train, Jasper National Park, Alberta, M.S. thesis, Univ. of Alberta, Edmonton, Canada, 1979.

Richards, J. A., P. W. Woodgate, and A. K. Skidmore, An explanation of enhanced radar backscattering from flooded forests, *Int. J. Remote Sens.*, *8*, 1093–1100, 1987.

Robertson-Rintoul, M. S. E., and K. S. Richards, Braided-channel pattern and paleohydrology using an index of total sinuosity, in *Braided Rivers*, edited by J. L. Best and C. S. Bristow, *Geol. Soc. Spec. Publ.*, *75*, 113–118, 1993.

Sippel, S. J., S. K. Hamilton, and J. M. Melack, Inundation area and morphometry of lakes on the Amazon River floodplain, Brazil, *Arch. Hydrobiol.*, *123*, 385–400, 1992.

Sippel, S. J., S. K. Hamilton, J. M. Melack, and B. J. Choudhury, Determination of inundation area in the Amazon River floodplain using the SMMR 37 GHz polarization difference, *Remote Sens. Environ.*, *48*, 70–76, 1994.

Slatt, R. M., and C. M. Hoskin, Water and sediment in the Norris Glacier outwash area, upper Taku inlet, southeastern Alaska, *J. Sediment. Petrol.*, *38*(2), 434–456, 1968.

Smith, L. C., Satellite remote sensing of river inundation area, stage, and discharge: A review, *Hydrol. Process.*, in press, 1996.

Smith, L. C., B. L. Isacks, R. R. Forster, A. L. Bloom, and I. Preuss, Estimation of discharge from braided glacial rivers using ERS 1 SAR: First results, *Water Resour. Res.*, *31*(5), 1325–1329, 1995.

Tholey, N., Monitoring flood events with remote sensing data: An example of ERS-1's contribution to flood events in northern and southern France regions, paper presented at First Thematic Working Group Meeting on Flood Monitoring, ESRIN/Eur. Space Agency, Frascati, Italy, June 26–27, 1995.

A. L. Bloom and B. L. Isacks, Institute for the Study of Continents, Department of Geological Sciences, Snee Hall, Cornell University, Ithaca, NY 14853-1504.

A. B. Murray, Scripps Institution of Oceanography, University of California, San Diego, La Jolla, CA 92093. (e-mail: brad@bagnold.ucsd.edu)

L. C. Smith, Department of Geography, University of California, Los Angeles, CA 90095. (e-mail: lsmith@geog.ucla.edu)

(Received September 28, 1995; revised February 26, 1996; accepted March 5, 1996.)